

Generalized Many-Body Dispersion Correction through Random-phase Approximation for Chemically Accurate Density Functional Theory

Pier Paolo Poier,^{*,†} Louis Lagardère,^{†,‡} and Jean-Philip Piquemal^{*,†,¶}

[†]*Sorbonne Université, LCT, UMR 7616 CNRS, Paris, France*

[‡]*Sorbonne Université, IP2CT, FR 2622 CNRS, Paris, France*

[¶]*The University of Texas at Austin, Department of Biomedical Engineering, TX, USA*

E-mail: pier.poier@sorbonne-universite.fr; jean-philip.piquemal@sorbonne-universite.fr

Abstract

We extend our recently proposed Deep Learning-aided many-body dispersion (DNN-MBD) model to quadrupole polarizability (Q) terms using a generalized Random Phase Approximation (RPA) formalism enabling to include van der Waals contributions beyond dipole. The resulting DNN-MBDQ model only relies on *ab initio*-derived quantities as the introduced quadrupole polarizabilities are recursively retrieved from dipole ones, in turn modelled via the Tkatchenko-Scheffler method. A transferable and efficient deep-neuronal network (DNN) provides atom in molecule volumes, while a single range-separation parameter is used to couple the model to Density Functional Theory (DFT). Since it can be computed at negligible cost, the DNN-MBDQ approach can be coupled with DFT functionals such as as PBE/PBE0 or B86bPBE(dispersionless). DNN-MBDQ-PBE/PBE0 reaches chemical accuracy exhibiting superior accuracy compared to other dispersion-corrected models, especially at

near-equilibrium ranges where errors are lowered by nearly 25% compared to our dipole-only approach while gains reach nearly 50% compared to other corrected schemes.

Introduction

The importance of modelling matter through computer simulations has risen tremendously in the past decades in virtue of both the theoretical achievements and the advent of mass-produced computers whose performances have increased exponentially. Despite these tremendous achievements, the exact solution of the non-relativistic electronic Schrödinger equation remains out of reach for multi-electron systems and different approximations have been introduced in order to model and tackle systems of chemical relevance. In particular, Kohn-Sham Density Functional Theory (KS-DFT) has established itself the most widely used electronic structure method being the cheapest way for introducing electronic correlation. KS-DFT is based on the idea of evaluating the kinetic energy from a single Slater determinant, thus assuming the electrons being non-interacting. The difference between the true and KS kinetic energies as well as the difference between the true electronic and exchange interaction ones is essentially embedded and modelled by the exchange correlation functional, key quantity in KS-DFT, however, in practice unknown.

The different approaches taken in modelling of the exchange-correlation functional define the plethora of KS-DFT variants which, however, are mainly capable of capturing local correlation effects. Dispersion interactions, on the other hand, are rooted in the long-range electron correlation that can clearly not be captured by the intrinsic locality of common exchange correlation functionals. This inadequacy of KS-DFT in modelling non-covalent dispersion interactions, ubiquitous in nature and materials, has risen the attention towards the development of dispersion correction models,¹ the most widely used

being based on empirical pairwise terms, Eq.(1).²

$$\mathcal{E}_{\text{disp}} = \sum_{i>j}^N -\frac{C_6^{ij}}{R_{ij}^6} \quad (1)$$

This pairwise approach coupled with KS-DFT has shown to provide very good accuracy despite its very simple nature that adds basically negligible computational time and for this reason it is also employed in the majority of force fields as the attractive component of the Lennard-Jones potential.

Each of the pairwise terms above can be further expanded via a second-order perturbative approach³ (in the limit of large inter-atomic separation) to include the higher-order contributions shown in Eq.(2) where $\alpha_k^j(i\nu)$ is the k -pole polarizability at imaginary frequency of atom j (only the single pair ij is considered for the sake of simplicity).⁴

$$\begin{aligned} \mathcal{E}_{\text{disp}} &= -\frac{C_6^{ij}}{R_{ij}^6} - \frac{C_8^{ij}}{R_{ij}^8} - \frac{C_{10}^{ij}}{R_{ij}^{10}} - \dots \\ C_{2n}^{ij} &= \frac{(2n-2)!}{2\pi} \sum_{h=1}^{n-2} \frac{1}{(2h)!(2k)!} \int_0^\infty d\nu \alpha_h^i(i\nu) \alpha_k^j(i\nu) \quad , \quad k = n - h - 1 \end{aligned} \quad (2)$$

While providing the correct long-range asymptotic limit, C_6 terms alone are not enough to describe the short and medium range dispersion effects and these higher-order terms have proven to increase significantly interaction energies near equilibrium regions as well as condensed phase properties obtained with molecular dynamics simulations based on force field potentials.⁵

Regardless of the higher-order terms inclusion discussed, this pairwise approach completely neglects the collective many-body dispersion (MBD) effects inherited from the intrinsic quantum mechanical nature of long-range electron correlation and their relevance has been proven in modelling extended systems, supramolecular complexes and proteins in solutions.⁶⁻⁹

These non-additive dispersion effects have been modelled via a set of coupled fluctuating

dipoles^{10,11} as well as quantum Drude oscillators.¹² In recent years, Tkatchenko, DiStasio Jr. and Ambrosetti have proposed the MBD@rsSCS introducing the range-separation of the self-consistent screening (rsSCS) of atomic polarizabilities based on Tkatchenko-Scheffler volume rescaling that relies on the molecular electron density.¹³ This many-body dispersion approach is particularly elegant as it fully relies on *ab initio*-derived parameters (atomic polarizabilities) except for the unique range separation parameter governing the coupling to the chosen KS-DFT method while providing chemical accuracy.¹³

Being based on the interaction among coupled fluctuating dipoles, the MBD model (rsSCS is implicitly assumed and from now dropped) represents the many-body counterpart of Eq.1 where the effect of higher-order fluctuating multipoles are neglected. In this work we will generalize the MBD model to coupled fluctuating dipole and quadrupoles in order to improve the description of short and mid-range many-body dispersion. Particularly, we will show how atomic quadrupole polarizabilities can be recursively derived from dipole ones, thus without the need on introducing further parameters. In doing so we will adopt our recently proposed deep neuronal network (DNN) model approach completely bypassing the explicit electron density partitioning. The outcoming density-free DNN-MBDQ model exhibits improved accuracy especially near equilibrium regions without the inclusion of any additional parameter, outperforming other many-body dispersion models.

Theory

The correlation energy \mathcal{E}_c for a system of interacting electrons can be rigorously expressed with the adiabatic connection fluctuation-dissipation formula, χ_λ and χ_0 being the interacting and non-interacting response functions, v is the Coulomb potential $|\mathbf{r} - \mathbf{r}'|^{-1}$ and λ its coupling strength.

$$\mathcal{E}_c = -\frac{1}{2\pi} \int_0^\infty d\nu \int_0^1 d\lambda \text{Tr} [\chi_\lambda(\mathbf{r}, \mathbf{r}', i\nu) - \chi_0(\mathbf{r}, \mathbf{r}', i\nu)v(\mathbf{r}, \mathbf{r}')] \quad (3)$$

By completely neglecting the exchange-correlation kernel dependence on λ , it is possible to introduce the random phase approximation (RPA) form of χ_λ , Eq.(4) perform the λ -integration analytically and this gives rise to the RPA correlation energy in Eq.(5) where the frequency and position dependence are dropped for simplicity while the explicit χ_0 expression in terms of orbital functions and energies can be found in reference.¹⁴

$$\chi_\lambda(\mathbf{r}, \mathbf{r}', i\nu) = \frac{\chi_0(\mathbf{r}, \mathbf{r}', i\nu)}{1 - \chi_0(\mathbf{r}, \mathbf{r}', i\nu)v(\mathbf{r}, \mathbf{r}')} \quad (4)$$

$$\mathcal{E}_c^{\text{RPA}} = \frac{1}{2\pi} \int_0^\infty d\nu \text{Tr} [\ln(1 - \chi_0 v) + \chi_0 v] \quad (5)$$

In virtue of its generality, this framework here introduced for the case of electronic correlation, can be used in different contexts and in particular in connection with the many-body dispersion model where the target energy arises from the correlation of coupled fluctuating dipoles.¹⁵ In this case the response function assumes the form of the frequency-dependent atom-in-molecule (AIM) isotropic dipole polarizability $\alpha_i^\mu(i\nu)$ localized at the atomic position R_i while the Coulomb potential $v(\mathbf{r}, \mathbf{r}')$ is replaced by the (properly damped) dipole-dipole interaction tensor $\mathbf{T}_{ij}^{\text{LR}} = \mathbf{T}_{ij}^{\text{LR},\mu\mu}$.

Eq.(5) is thus written in terms of the MBD model's quantities as shown in Eq.(6), $\mathbf{A}(i\nu)$ being the diagonal superpolarizability matrix defined as $\text{Diag}[\alpha_1^\mu(i\nu), \alpha_2^\mu(i\nu), \dots, \alpha_N^\mu(i\nu)]$ and \mathbf{T}^{LR} being the full dipole-dipole interaction tensor excluding self interactions ($\mathbf{T}_{ii}^{\text{LR}} = \mathbf{0}$). We note that Eq.(6) does not include the $\chi_0 v$ term appearing in Eq.(5) due to the traceless property of the $\mathbf{A}(i\nu)\mathbf{T}^{\text{LR}}$ matrix product.

$$\mathcal{E}_{\text{MBD}} = \frac{1}{2\pi} \int_0^\infty d\nu \text{Tr} [\ln(\mathbf{I} - \mathbf{A}(i\nu)\mathbf{T}^{\text{LR}})] \quad (6)$$

For MBD models based on coupled fluctuating dipoles, the RPA formula in Eq.(6)

does not represent the most efficient strategy to compute correlation energies solution as the problem can be equivalently solved via exact diagonalization of the MBD potential matrix for a system of coupled quantum harmonic oscillators.¹⁵ However, the power and generality of the RPA formulation of the MBD model allows for the generalization of the model and the inclusion of higher-order polarizabilities as discussed below.

The matrix form of Eq.(6) can rather straightforwardly be generalized to higher-order moments gathered in $\mathbf{A}(iv)$ by consistently augmenting the interaction tensor \mathbf{T} with proper interaction blocks. In particular, for a model based on coupled fluctuating dipoles and quadrupoles (Q), the two matrices of dimension $(12N, 12N)$, N being the number of atoms in the systems, take the form reported in Eq.(7) where a general out-of-diagonal (thus non-vanishing) block of size $(12, 12)$ is shown.

$$\mathbf{A}_{kk}(iv) = \mathbf{Diag}[\alpha_k^\mu(iv), \alpha_k^\mu(iv), \alpha_k^\mu(iv), \alpha_k^Q(iv), \alpha_k^Q(iv), \alpha_k^Q(iv), \dots, \alpha_k^Q(iv)]$$

$$\mathbf{T}_{ik}^{\text{LR}} = \left(\begin{array}{c|c} \mathbf{T}_{ik}^{\text{LR},\mu\mu} & \mathbf{T}_{ik}^{\text{LR},\mu Q} \\ \hline \mathbf{T}_{ik}^{\text{LR},\mu Q} & \mathbf{T}_{ik}^{\text{LR},QQ} \end{array} \right) , \quad i \neq k \quad (7)$$

We will now focus our attention on \mathbf{A} and in particular in its dipole and quadrupole dynamic polarizability entries being the model's key parameters.

As mentioned earlier, a pleasant feature of the MBD model is the fact that it only relies on *ab initio*-derived parameters. In particular, AIM dipole polarizabilities are typically obtained via the Tkatchenko-Scheffler (TS) volume rescaling approach shown in Eq.(8), α_i^μ and V_i being the TS static dipole polarizability and AIM volume respectively of the i -th

atom while the zero superscript denotes free-atom reference quantities.

$$\alpha_i^\mu(0) = \left(\frac{V_i}{V_i^0} \right) \alpha_i^{\mu,0}(0) \quad (8)$$

The AIM volume V_i is typically obtained by Hirshfeld partitioning the explicit electron density obtained via the solution of KS equations. However, we have recently proposed an efficient 5-hidden layers DNN model trained with the minimal basis iterative Stockholder atom¹⁶ (MBISA) volumes of approximately 4.6 millions molecules capable of providing AIM volumes bypassing the electron density partitioning.¹⁷ Based on its accuracy and transferability, we will employ our DNN model to retrieve AIM volumes, however, the following discussion remains valid also with explicit density partitioning schemes.

The next step is to find a suitable and reliable expression for $\alpha_i^Q(0)$, possibly without the introduction of empirical parameters. We note, at this point, that it is possible to relate two consecutive dispersion coefficients by the recursive relation shown in Eq.(9) for the specific case of homonuclear C_6^{ii} and C_8^{ii} coefficients, where Z_i is the atomic number, $\langle r^n \rangle$ are expectation values or multipole-type moments derived from atomic densities while γ scaling factor will be introduced shortly.¹⁸

$$\begin{aligned} C_8^{ii} &= 3C_6^{ii}Q_i \\ Q_i &= \gamma \sqrt{Z_i} \frac{\langle r^4 \rangle_i}{\langle r^2 \rangle_i} \end{aligned} \quad (9)$$

We can now assume to model atom i via a quantum Drude particle characterized by the frequency ω_i and thus express C_6^{ii} and C_8^{ii} in terms of dipole and quadrupole polarizability, Eqs.(10) and (11).¹⁹

$$C_6^{ii} = \frac{3}{4} \omega_i [\alpha_i^\mu(0)]^2 \quad (10)$$

$$C_8^{ii} = 5\omega_i \alpha_i^\mu(0) \alpha_i^Q(0) \quad (11)$$

Finally, by inserting Eqs.(10) and (11) in Eq.(9), one obtains the static AIM quadrupole

polarizability in Eq.(12).

$$\alpha_i^Q(0) = \frac{9}{20} Q_i \alpha_i^\mu(0) \quad (12)$$

The γ scaling factor is modelled similarly to Carter-Fenk *et al.*, Eq.(13), in particular γ^0 is chosen such that noble-gas quadrupole polarizabilities are reproduced.²⁰

$$\gamma = \gamma_0 + \exp(-\sqrt{Z_i}/2) \quad (13)$$

The above discussed recursive relation represents an efficient strategy to derive quadrupole polarizabilities that can be readily applied to any AIM volume partitioning scheme as the atomic volume is the only density-related quantity which, however, in this work is retrieved from an accurate DNN model.

The solution of Eq.(6) requires frequency-dependent atomic polarizabilities while our discussion was, until now, restricted to the zero-frequency (static) case.

Dynamical dipole polarizabilities have been successfully modelled via a [0/2] Padé approximant form and Tang *et al.* suggested the same form to be employed also in modelling higher-order multipole dynamical polarizabilities, as shown in Eq.(14), the superscript $2m$ denoting a general multipole level and $\omega_j^{2m,0}$ the free-atom multipolar-dependent characteristic excitation frequency.²¹

$$\alpha_k^{2m}(\mathrm{i}\nu) = \frac{\alpha_k^{2m,0}(0)}{1 - (\mathrm{i}\nu/\omega_k^{2m,0})^2} \quad (14)$$

In particular, we employ a common $\omega_k^{2m,0}$ parameter for both dipole and quadrupole dynamical polarizabilities and we express it as a function of free atom C_6 and static dipole polarizability, Eq.(15).

$$\omega_k^{Q,0} = \omega_k^{\mu,0} = \frac{4}{3} \frac{C_6^{0,kk}}{[\alpha_k^{2m,0}(0)]^2} \quad (15)$$

This assumption is, however, well defined as it guarantees to model dynamical quadrupole

polarizabilities as lower bound quantities while the introduction of *ab initio*-derived scaling factors could be used to improve over this assumption.²¹

We note that the dipole polarizabilities used in Eq.(12), can be either taken directly from Eq.(8) or can be further screened by solving Dyson-like self-consistent screening equations.^{13,22} In this work the latter is chosen and, as a consequence, these screening effects are thus transferred to quadrupole polarizabilities via Eq.(12).

The explicit expressions of the multipole interaction tensor $\mathbf{T}_{ik}^{\text{LR}}$, is given in Eq.(16) for the ik pair placed at distance R_{ik} and greek letters are used to denote x, y, z Cartesian components while the damping function is shown separately in Eq.(17).

$$\begin{aligned}\mathbf{T}_{ik,\tau\sigma}^{\text{LR},\mu\mu} &= f(R_{ik}, S_{ik}) \nabla_{ik,\tau\sigma}^2 \left(\frac{1}{R_{ik}} \right) \\ \mathbf{T}_{\tau\sigma\theta}^{\text{LR},\mu Q} &= f(R_{ik}, S_{ik}) \nabla_{ik,\tau\sigma\theta}^3 \left(\frac{1}{R_{ik}} \right) \\ \mathbf{T}_{ik,\tau\sigma\theta\lambda}^{\text{LR},QQ} &= f(R_{ik}, S_{ik}) \nabla_{ik,\tau\sigma\theta\lambda}^4 \left(\frac{1}{R_{ik}} \right)\end{aligned}\quad (16)$$

The Fermi damping function $f(R_{ik}, S_{ik})$ defined in Eq.(17) where R_i^{vdw} represents the AIM van der Waals radius obtained as the ratio between the AIM dipole (screened) polarizability and the free atom one while β is the parameter modulating the range-separation of the multipole interaction tensor.

$$\begin{aligned}f(R_{ik}, S_{ik}) &= \frac{1}{1 + \exp(-6(R_{ik}/S_{ik} - 1))} \\ S_{ik} &= \beta(R_i^{\text{vdw}} + R_k^{\text{vdw}}) \\ R_i^{\text{vdw}} &= \left(\frac{\alpha_i^\mu(0)}{\alpha_i^{\mu,0}(0)} \right)^{1/3} R_i^{0,\text{vdw}}\end{aligned}\quad (17)$$

As it appears in Eq.(16), all dipole-dipole, quadrupole-quadrupole and mixed terms are screened by a common damping function. This may not be the most optimal solution for

shorter-range interaction regimes as different multipolar interactions could be modelled by specific damping terms in line to what discussed by Tang and Toennies,²³ however, in virtue of its simplicity, this approach will be embraced in this work.

We solve the RPA formula in Eq.(6) by means of Gauss-Legendre, nevertheless, more sophisticated quadrature techniques such as the Clenshaw-Curtis quadrature^{24,25} could also be potentially employed.

The DNN-MBDQ model is implemented in the Tinker-HP package²⁶ where the extremely efficient linear-scaling stochastic Lanczos-based DNN-MBD model is also implemented.²⁷ PBE and PBE0 pure energies have been calculated with Jensen's pcseg-3 basis set as it corresponds *de facto* to the complete basis set limit for the employed semi-local functionals.²⁸

Results

The above described DNN-MBDQ model is tested in connection to PBE and PBE0 density functionals as this allows for a ready comparison with ready available literature including the dipole-only DNN-MBD model. The usual S66x8 dataset for noncovalent biologically relevant interactions²⁹ consisting of 66 dimers placed at 8 different inter-molecular distances (CCSD(T) complete basis set interaction energies) was taken as reference to tune the β parameter in Eq.(17) for the two functional chosen and the optimal values are shown in Table 1 together with the ones relative to the dipole-only based DNN-MBD.

Table 1: Range-separation β parameter values optimized by minimizing the mean absolute relative error for the DNN-MBD and DNN-MBDQ models coupled with the PBE and PBE0 functionals for the S66x8 data set.

DFT functional	DNN-MBD	DNN-MBDQ
PBE	0.75	0.84
PBE0	0.77	0.85

We observe that the PBE0/DNN-MBDQ method requires a larger range-separation parameter compared to the correspondent PBE-based model. This is consistent to what

observed also in the PBE/DNN-MBD model due to the PBE0 functional's improved description of short-range exchange-correlation.

Moreover, the DNN-MBDQ model requires larger range-separation parameters compared to the DNN-MBD one, and this can be rationalized in virtue of the additional stabilizing dispersion contributions arising from the dipole-quadrupole and quadrupole-quadrupole interactions being the many-body analogues of the pairwise C_8 and C_{10} terms in Eq.(2). It is now of interest to compare the DNN-MBDQ error for the present dataset with the ones related to different dipole-only MBD models, Tab.2.

Table 2: MAE (kcal/mol) and MARE(%) relative to the S66x8 data set for our density free DNN-MBD and DNN-MBDQ models as well as few other dipole-only MBD models coupled with the PBE and PBE0 functionals. MAE and MARE are computed.

Model	MAE[kcal/mol]	MARE%
PBE	1.55	65
PBE/D3	0.44	n.a.
PBE/MBD@rsSCS ¹³	0.32	10.6
PBE/MBD@rsSCS/FI ³⁰	0.28	9.0
PBE/DNN-MBD ¹⁷	0.25	9.0
PBE+DNN-MBDQ	0.24	11.0
PBE0	1.48	65
PBE0/MBD@rsSCS	0.30	9.2
PBE0/DNN-MBD	0.23	6.9
PBE0/DNN-MBDQ	0.21	8.5

The proposed DNN-MBDQ model exhibits reduced mean absolute errors, although by a small margin, compared to its dipole-only based DNN-MBD version coupled with both PBE0 and PBE functionals while compared to other MBD-corrected models the lower errors, remain marked. Even in the case of the DNN-MBDQ, dispersion corrected PBE0 provides the smallest error for the considered S66x8 dataset, in line to what observed in the DNN-MBD as well as other dipole-only MBD models.

Very recently, we became aware that a beyond-dipole MBD model including quadrupolar effects and denominated MBD+Q@rsSCS was also proposed by Massa, Ambrosetti and Silvestrelli.³¹ In their approach the coupled quantum harmonic oscillators modelling

many-body dispersion are parametrized by a mixed approach based on both the Tkatchenko-Scheffler polarizability rescaling and Johnson' exchange dipole model.³² This differs substantially from our approach where quadrupole polarizabilities are simply obtained recursively from dipole ones, in turn derived from our DNN-based Tkatchenko-Scheffler polarizability scheme. Table 3 directly compares the MBD+Q@rsSCS and our DNN-MBDQ model based on the complete S66x8 dataset, the S66x7 subset where the shortest inter-molecular distances are disregarded as well as the S66 dataset.

Table 3: MBD+Q@rsSCS and DNN-MBDQMBD methods compared in terms of mean absolute errors (kcal/mol) while MARE are reported in brackets for the S66, S66x7 and S66x8 datasets. **# params** denotes the number of parameters optimized in the damping function against the S66x8 set for each of the proposed methods.

Model	# params	S66	S66x7	S66x8
PBE/MBD+Q@rsSCS	2	0.45 (9.3%)	0.27 (7.6%)	0.34 (12.0%)
PBE/DNN-MBDQ	1	0.24 (5.5%)	0.20 (10.2%)	0.24 (11.0%)
PBE0/MBD+Q@rsSCS	2	0.28 (11.8%)	0.22 (7.1%)	0.37 (8.3%)
PBE0/DNN-MBDQ	1	0.22 (4.1%)	0.18 (7.5%)	0.21 (8.5%)

In all the data sets considered, and for both PBE and PBE0 cases, the DNN-MBDQ consistently exhibits lower (in some cases by nearly 50%) MAE compared to MBD+Q@rsSCS one despite the latter relies on the optimization of two range-separation parameters while a single parameter is optimized for our DNN-MBDQ model. In both models, the removal of the shortest inter-molecular distance (S66x7) involves a lowering of the error compared to the full S66x8 set and this can be attributed to the shared damping function employed for all the multipolar interaction blocks as discussed by Massa *et al.*, and this is common to both the MBD+Q@rsSCS and DNN-MBDQMBD models.³¹

The dipole contribution to dispersion interactions dominates the long-range asymptotic limit while inclusion of quadrupole contributions improves the description at medium ranges near equilibrium distances. The S66x8 is an optimal dataset to optimize the range-separation parameters as it is not biased towards equilibrium distances. However, in virtue of its wide range of inter-molecular distances, it does not represent a fully optimal

set to investigate the effects of quadrupole terms. In that regard, results on the S22 dataset, which is composed of model complexes at equilibrium distances, are a better judge of the accuracy of our model since S22 includes more interactions in the full quadrupole (and mixed dipole-quadrupole) operational regime. Therefore, the S22 validation set enables us to better understand the effects of the added quadrupole terms as well as to investigate the transferability of the DNN-MBDQ model by employing the same range-separation parameters reported in Table (1).

Table 4: MAE (kcal/mol) and MARE(%) relative to the S22 data set for some dipole-only based MBD models as well as for our DNN-MBDQ model. For the MBD-based models, the range-separation parameter was optimized against the S66x8 dataset. Revised S22 energies are taken in computing MAE and MARE values.³³

Model	MAE[kcal/mol]	MARE%
PBE	2.66	58
PBE/D3	0.48	n.a.
PBE/MBD@rsSCS	0.49	8.9
PBE/DNN-MBD	0.41	6.6
PBE/DNN-MBDQ	0.29	6.1
PBE0	2.44	55
PBE0/MBD@rsSCS	0.55	8.5
PBE0/DNN-MBD	0.43	5.6
PBE0/DNN-MBDQ	0.30	6.1

Table 4 shows the performances of different dispersion correction models including the DNN-MBDQ for the S22 data set. Compared to the S66x8 case where the accuracy gain introduced by the DNN-MBDQ model is contained, for the S22 test set the MAE is reduced by 30% compared to the already dipole-only DNN-MBD (both PBE and PBE0) while, if compared to the MBD@rsSCS model coupled with the PBE and PBE0, the MAE decreases by 41% and 45% respectively. These noteworthy performances stem certainly from the additional quadrupolar terms as this is readily observed by a direct comparison between the DNN-MBD and DNN-MBDQ models. The pleasant recursive relation for quadrupole polarizabilities, Eq.(12), benefits from the DNN model's AIM volumes accuracy arising from the minimal basis stockholder atom data used in the training process,

whose better properties, compared to the common Hirshfeld partitioning, have been discussed in references.^{16,17}

The DNN-MBDQ model coupled with the PBE and PBE0 functionals provides one of the lowest errors for the S22 set without an *ad hoc* parameter optimization. This is rather significant considering that the model fully relies on *ab initio* quantities and its coupling to the target functional is determined by a single range-separation parameter optimized for the S66x8 set, thus including out-of-equilibrium geometries. Close performances have been obtained with B3LYP-DCP and PW6B95-D3 methods which, however, rely on a large number of empirical parameters while not including many-body dispersion effects.¹ The accuracy performances of the DNN-MBDQ mode could be potentially increased further by adding an extra parameter in the Fermi function (Eq.(17)), as well as by employing different forms of it for the dipole-dipole, dipole-quadrupole and quadrupole-quadrupole interaction blocks and future efforts will be spent in this direction.

In order to design an accurate and reliable dispersion-corrected KS-DFT model, both the functional and the dispersion correction must fulfill specific criteria. These requirements are essential for avoiding error cancellation effects in favor of more physically grounded achievement of small errors, as recently discussed by Price, Bryenton and Johnson.³⁴ While the dispersion correction should possibly include higher-order terms as well as many-body effects, the DFT functional should be dispersionless since by adding a dispersion correction to an exchange-correlation functional that somewhat partially includes dispersion, will lead to double counting at shorter ranges, with a consequent lost of accuracy. In fact, in order to reduce this artifact, dispersion corrections are often excessively damped with an inevitable deterioration of the mid-range interactions' description. Among the possible dispersionless functionals, the B86bPBE has proven numerically stable and, coupled with the exchange-hole dipole moment dispersion model,^{35,36} has performed well for molecular and material applications.³⁷

On account of both the higher-order terms and the many-body nature of the proposed

DNN-MBDQ dispersion correction, thus fulfilling the above mentioned criteria, it is of interest to probe its performances in connection with the B86bPBE dispersionless functional.

In doing so, we employ the S22 data set since, as mentioned earlier, the dimers placed at equilibrium distance allow us to better investigate the role of higher moments introduced with the DNN-MBDQ model. The range separation parameter is optimized to minimize the error, this time directly on the S22 set and the same is repeated for the PBE/DNN-MBDQ in order to make a fair comparison as well as for the dipole-only B86bPBE/DNN-MBD model, Table 5. First, we note that the B86bPBE/DNN-MBDQ requires a smaller

Table 5: MAE (kcal/mol) and MARE(%) relative to the S22 data set for the PBE and B86bPBE functionals respectively as well as their dispersion corrected form. This time the range-separation parameters were directly optimized against the S22 dataset and their values are reported in the second column.

Model	β	MAE[kcal/mol]	MARE%
PBE	n.a.	2.66	58
B86bPBE	n.a.	3.28	72
PBE/DNN-MBDQ	0.82	0.25	5.2
B86bPBE/DNN-MBD	0.68	0.49	10
B86bPBE/DNN-MBDQ	0.78	0.37	9.9

range-separation parameter (less damping) compared to its PBE counterpart. This is completely in line with the less stabilizing nature of the B86bPBE functional arising from its almost dispersion-free features as shown in Figure 1 for the argon dimer. In fact, a less damped DNN-MBDQ correction leads to model dispersion at shorter ranges where functionals such as PBE and PBE0 usually involve more damped dispersion corrections to avoid double counting. The β parameter obtained for the PBE/DNN-MBDQ is, compared to the one of the S66x8 data set, smaller in magnitude. This is rationalized in virtue of the shorter intermolecular distances involved by the S66x8 set for which, the pure functional is capable of modelling local correlation effects in the short-range regime thus requiring a larger damping of the DNN-MBDQ model.

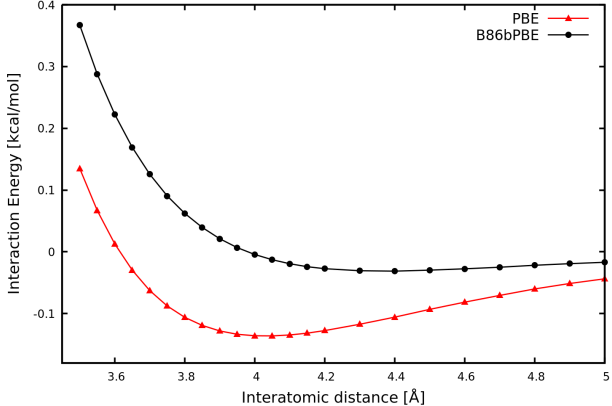


Figure 1: Interaction energy for the argon dimer computed with the PBE and B86bPBE pure functionals (pcseg-3 basis set) as a function of the interatomic distance.

The error (S22) relative to the B86bPBE/DNN-MBDQ model is 0.37 kcal/mol, larger than the very low 0.25 kcal/mol error given by the PBE/DNN-MBDQ, however, markedly smaller compared to dipole-only MBD-corrected DFT models and, in any case, abundantly below the chemical accuracy limit of 1 kcal/mol. Even in the case of the B86bPBE functional employed, the DNN-MBDQ correction involves a smaller error compared to the dipole-only DNN-MBD counterpart, thus confirming the importance of quadrupolar effects in mid-ranged interactions distances, confirming what observed and discussed for the PBE/PBE0 functionals. The bottleneck in the accuracy related to the use of B86bPBE/DNN-MBDQ model is most likely to be addressed to the inadequacy of a semi-classical treatment of dispersion at short to mid-ranges as it is implied by the smaller range-separation parameter involved. In fact, at this regime, the long-range correlation that manifests itself as dispersion, smoothly turns into local electron correlation whose description should be better modelled by the density functional, especially at shorter ranges, Figure 2. This aspect could be ameliorated by developing a suitable hybrid component to the B86bPBE functional capable of improving the description of short/mid interaction ranges, therefore leaving to the MBD correction the purely dispersive mid/long-ranged interaction regimes.

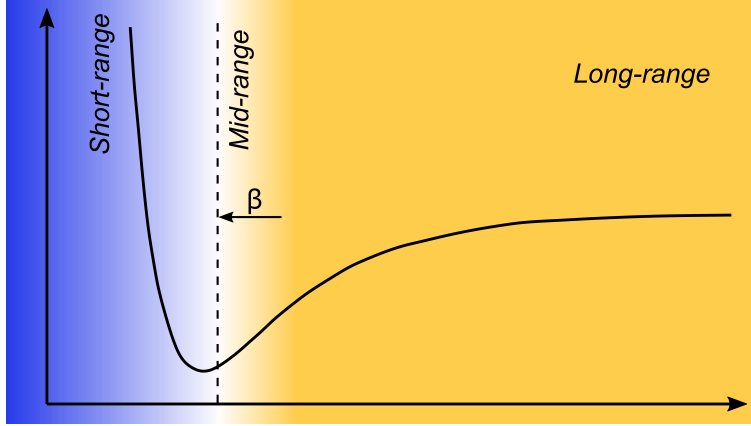


Figure 2: Pictorial representation of the short-, mid- and long-range interaction regimes. The dashed line represents the transition between the short-range part modelled by the KS-DFT functional (blue) and the long-range (yellow) regimes modelled by the DNN-MBD dispersion correction where the introduced quadrupoles improve the modelling of mid-ranges near equilibrium distances. Smaller β parameters required by dispersionless functionals have the effect of pushing the yellow zone toward shorter ranges.

Conclusions

We propose the DNN-MBDQ model where the density-free/deep learning-aided many-body dispersion model is extended to quadrupolar polarizability terms thanks to a Random Phase Approximation formalism. Quadrupole polarizabilities are recursively retrieved from free-atom dipole polarizabilities and atom-in-molecule volumes modelled via the accurate and transferable neuronal network recently proposed.¹⁷ The proposed strategy can be readily applied to MBD model based on the volume rescaling polarizability partitioning as it does not require any additional electron density-derived quantity. The density-free DNN-MBDQ model implemented in the Tinker-HP package exhibits improved accuracy compared to dipole-based MBD models. In particular, for the equilibrium inter-molecular distances covered by the widely used S22 data set, the DNN-MBDQ shows a remarkable improvement (up to 45%) compared to dipole-only based MBD models and this highlights the importance of quadrupole-quadrupole and dipole-quadrupole interaction contributions at mid-ranges.

The DNN-MBDQ model was also coupled with the B86bPBE dispersionless functional,

resulting in lower errors compared to the case where the dipole-only DNN-MBD correcc-tion was employed, confirming the important role of quadrupoles.

We believe that the high accuracy exhibited by the DNN-MBDQ model coupled with semi-local functionals will be beneficial in pushing Kohn-Sham Density Functional Theory a step closer to post-Hartree Fock reference standards which, due to their high computational cost can not be employed to explore larger systems of relevance in bio- and material modelling. Further work will be therefore dedicated to the evaluation of possible couplings of the DNN-MBDQ approach with existing modern DFT functionals towards generalized chemical accuracy. Such a strategy opens the door to designing accurate, large-scale, energies databases towards various machine learning applications. Finally, the DNN-MBDQ energy correction can be directly added as an *a posteriori* term to pure KS-DFT energies in virtue of the model's density-free features arising from the transferable deep neuronal network employed.

Acknowledgement

This work has been funded by the European Research Council (ERC) under the European Union's Horizon 2020 research and innovation program (grant No 810367), project EMC2 (JPP). Computations have been performed at GENCI (IDRIS, Orsay, France and TGCC, Bruyères le Chatel) on grant no A0070707671.

Supporting Information Available

References

- (1) Grimme, S.; Hansen, A.; Brandenburg, J. G.; Bannwarth, C. Dispersion-corrected mean-field electronic structure methods. *Chemical Reviews* **2016**, *116*, 5105–5154.

(2) Grimme, S. Accurate description of van der Waals complexes by density functional theory including empirical corrections. *Journal of Computational Chemistry* **2004**, *25*, 1463–1473.

(3) Stone, A. *The Theory of Intermolecular Forces*, 2nd ed.; Oxford: Oxford, UK, 2013.

(4) Patil, S. H.; Tang, K. T. Multipolar polarizabilities and two- and three-body dispersion coefficients for alkali isoelectronic sequences. *The Journal of Chemical Physics* **1997**, *106*, 2298–2305.

(5) Visscher, K. M.; Geerke, D. P. Deriving a Polarizable Force Field for Biomolecular Building Blocks with Minimal Empirical Calibration. *The Journal of Physical Chemistry B* **2020**, *124*, 1628–1636.

(6) Reilly, A. M.; Tkatchenko, A. Seamless and accurate modeling of organic molecular materials. *The Journal of Physical Chemistry Letters* **2013**, *4*, 1028–1033.

(7) Ambrosetti, A.; Alfè, D.; DiStasio, R. A.; Tkatchenko, A. Hard numbers for large molecules: toward exact energetics for supramolecular systems. *The Journal of Physical Chemistry Letters* **2014**, *5*, 849–855.

(8) Ambrosetti, A.; Ferri, N.; DiStasio, R. A.; Tkatchenko, A. Wavelike charge density fluctuations and van der Waals interactions at the nanoscale. *Science* **2016**, *351*, 1171–1176.

(9) Stöhr, M.; Tkatchenko, A. Quantum mechanics of proteins in explicit water: the role of plasmon-like solute-solvent interactions. *Science Advances* **2019**, *5*, eaax0024.

(10) Langbein, D. Microscopic calculation of macroscopic dispersion energy. *Journal of Physics and Chemistry of Solids* **1971**, *32*, 133–138.

(11) Donchev, A. G. Many-body effects of dispersion interaction. *The Journal of Chemical Physics* **2006**, *125*, 074713.

(12) Jones, A. Quantum drude oscillators for accurate many-body intermolecular forces. Ph.D. thesis, University of Edinburgh, 2010.

(13) Ambrosetti, A.; Reilly, A. M.; DiStasio, R. A.; Tkatchenko, A. Long-range correlation energy calculated from coupled atomic response functions. *The Journal of Chemical Physics* **2014**, *140*, 18A508.

(14) Ren, X.; Rinke, P.; Joas, C.; Scheffler, M. Random-phase approximation and its applications in computational chemistry and materials science. *Journal of Materials Science* **2012**, *47*, 7447–7471.

(15) Tkatchenko, A.; Ambrosetti, A.; DiStasio, R. A. Interatomic methods for the dispersion energy derived from the adiabatic connection fluctuation-dissipation theorem. *The Journal of Chemical Physics* **2013**, *138*, 074106.

(16) Verstraelen, T.; Vandenbrande, S.; Heidar-Zadeh, F.; Vanduyfhuys, L.; Van Speybroeck, V.; Waroquier, M.; Ayers, P. W. Minimal basis iterative stockholder: atoms in molecules for force-field development. *Journal of Chemical Theory and Computation* **2016**, *12*, 3894–3912.

(17) Poier, P. P.; Jaffrelot Inizan, T.; Adjoua, O.; Lagardère, L.; Piquemal, J.-P. Accurate Deep Learning-Aided Density-Free Strategy for Many-Body Dispersion-Corrected Density Functional Theory. *The Journal of Physical Chemistry Letters* **2022**, *13*, 4381–4388, PMID: 35544748.

(18) Starkschall, G.; Gordon, R. G. Calculation of Coefficients in the Power Series Expansion of the Long-Range Dispersion Force between Atoms. *The Journal of Chemical Physics* **1972**, *56*, 2801–2806.

(19) Jones, A. P.; Crain, J.; Sokhan, V. P.; Whitfield, T. W.; Martyna, G. J. Quantum Drude oscillator model of atoms and molecules: Many-body polarization and dispersion interactions for atomistic simulation. *Phys. Rev. B* **2013**, *87*, 144103.

(20) Carter-Fenk, K.; Lao, K. U.; Liu, K.-Y.; Herbert, J. M. Accurate and Efficient ab Initio Calculations for Supramolecular Complexes: Symmetry-Adapted Perturbation Theory with Many-Body Dispersion. *The Journal of Physical Chemistry Letters* **2019**, *10*, 2706–2714.

(21) Tang, K. T.; Norbeck, J. M.; Certain, P. R. Upper and lower bounds of two- and three-body dipole, quadrupole, and octupole van der Waals coefficients for hydrogen, noble gas, and alkali atom interactions. *The Journal of Chemical Physics* **1976**, *64*, 3063–3074.

(22) Tkatchenko, A.; DiStasio, R. A.; Car, R.; Scheffler, M. Accurate and efficient method for many-body van der Waals interactions. *Phys. Rev. Lett.* **2012**, *108*, 236402.

(23) Tang, K. T.; Toennies, J. P. An improved simple model for the van der Waals potential based on universal damping functions for the dispersion coefficients. *The Journal of Chemical Physics* **1984**, *80*, 3726–3741.

(24) Eshuis, H.; Yarkony, J.; Furche, F. Fast computation of molecular random phase approximation correlation energies using resolution of the identity and imaginary frequency integration. *The Journal of Chemical Physics* **2010**, *132*, 234114.

(25) Mussard, B.; Rocca, D.; Jansen, G.; Ángyán, J. G. Dielectric Matrix Formulation of Correlation Energies in the Random Phase Approximation: Inclusion of Exchange Effects. *Journal of Chemical Theory and Computation* **2016**, *12*, 2191–2202, PMID: 26986444.

(26) Lagardère, L.; Jolly, L.; Lipparini, F.; Aviat, F.; Stamm, B.; Jing, Z. F.; Harger, M.; Torabifard, H.; Cisneros, G. A.; Schnieders, M. J.; Gresh, N.; Maday, Y.; Ren, P. Y.; Ponder, J. W.; Piquemal, J. P. Tinker-HP: a massively parallel molecular dynamics package for multiscale simulations of large complex systems with advanced point dipole polarizable force fields. *Chem. Sci.* **2018**, *9*, 956–972.

(27) Poier, P. P.; Lagardère, L.; Piquemal, J.-P. O(N) stochastic evaluation of many-body van der Waals energies in large complex systems. *Journal of Chemical Theory and Computation* **2022**, *18*, 1633–1645.

(28) Jensen, F. Unifying general and segmented contracted basis sets. Segmented polarization consistent basis sets. *Journal of Chemical Theory and Computation* **2014**, *10*, 1074–1085.

(29) Řezáč, J.; Riley, K. E.; Hobza, P. S66: A Well-balanced database of benchmark interaction energies relevant to biomolecular structures. *Journal of Chemical Theory and Computation* **2011**, *7*, 2427–2438.

(30) Gould, T.; Lebègue, S.; Ángyán, J. G.; Bučko, T. A fractionally ionic approach to polarizability and van der Waals many-body dispersion calculations. *Journal of Chemical Theory and Computation* **2016**, *12*, 5920–5930.

(31) Massa, D.; Ambrosetti, A.; Silvestrelli, P. L. Beyond-dipole van der Waals contributions within the many-body dispersion framework. *Electronic Structure* **2021**, *3*, 044002.

(32) Becke, A. D.; Johnson, E. R. Exchange-hole dipole moment and the dispersion interaction: High-order dispersion coefficients. *The Journal of Chemical Physics* **2006**, *124*, 014104.

(33) Takatani, T.; Hohenstein, E. G.; Malagoli, M.; Marshall, M. S.; Sherrill, C. D. Basis set consistent revision of the S22 test set of noncovalent interaction energies. *The Journal of Chemical Physics* **2010**, *132*, 144104.

(34) Price, A. J. A.; Bryenton, K. R.; Johnson, E. R. Requirements for an accurate dispersion-corrected density functional. *The Journal of Chemical Physics* **2021**, *154*, 230902.

(35) Becke, A. D.; Johnson, E. R. A density-functional model of the dispersion interaction. *The Journal of Chemical Physics* **2005**, *123*, 154101.

(36) Becke, A. D.; Johnson, E. R. Exchange-hole dipole moment and the dispersion interaction revisited. *The Journal of Chemical Physics* **2007**, *127*, 154108.

(37) Johnson, E. R. In *Non-covalent Interactions in Quantum Chemistry and Physics*; de la Roza, A. O., DiLabio, G., Eds.; Elsevier, 2017; pp 169–194.